Available online at www.sciencedirect.com

ScienceDirect

Mendeleev Commun., 2024, **34**, 902–904

Mendeleev Communications

Crystallization behavior of fluorozirconate glasses as monitored by ^{35}Cl NMR

Andrei A. Gippius,[a,b] Aleksei V. Tkachev,[a] Eleonora A. Kravchenko,[c] Leonid A. Vaimugin,[c] Liudmila V. Moiseeva[d] and Maria N. Brekhovskikh*[c]

[a] *P. N. Lebedev Physical Institute, Russian Academy of Sciences, 119991 Moscow, Russian Federation*
[b] *Department of Physics, M. V. Lomonosov Moscow State University, 119991 Moscow, Russian Federation*
[c] *N. S. Kurnakov Institute of General and Inorganic Chemistry, Russian Academy of Sciences, 119991 Moscow, Russian Federation. E-mail: mbrekh@igic.ras.ru*
[d] *Prokhorov General Physics Institute, Russian Academy of Sciences, 119991 Moscow, Russian Federation*

DOI: 10.1016/j.mencom.2024.10.042

The ^{35}Cl nuclear magnetic resonance (NMR) spectroscopy was first used to study the crystallization of erbium-doped fluorochlorozirconate glass in the ZrF_4–BaF_2–$BaCl_2$–LaF_3–AlF_3–NaF system. It has been shown that crystallization results in the increasing homogeneity of electronic structure on chlorine atoms and a narrowing of the NMR line. The glass being crystallized, erbium cations are displaced into the fluoride phase.

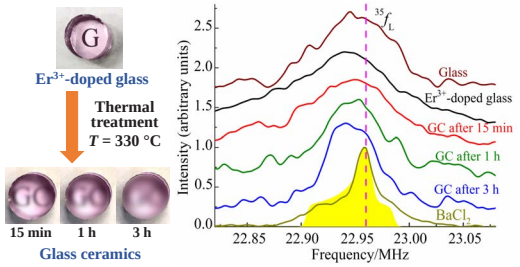

Keywords: fluorozirconate glass, crystallization, composition modification, glass ceramics, ^{35}Cl NMR spectroscopy, magnetic centers.

Fluorozirconate glass represents a promising optical media due to its low phonon energy,[1,2,3] which makes it attractive host for RE activators.[4] The luminescent properties of this material can be enhanced by modifying the glass composition with barium chloride and by heat treatment.[5] Fluorochloride glass ceramics are advanced materials for visualization in medical diagnostics,[1,6,7] non-destructive testing,[8,9] photovoltaics[10,11] and high-energy physics.[12] The changes in the intensity and the shape of the luminescence bands from erbium-doped fluorochloride glass were characterized for the Er^{3+} emitting transitions in the near and mid-IR region after heat treatment.[13] However, the nature of these changes as a function of temperature and time crystallization remains elusive. Therefore, when searching for optimal heat treatment conditions, it is necessary to select an appropriate physical chemical research method sensitive to the structural changes during the crystallization of fluorochlorozirconate glass. The methods of differential scanning calorimetry (DSC), transmission electron microscopy (TEM), X-ray diffraction (XRD), optical spectroscopy and Raman spectroscopy, provide scattered data and leave unresolved questions about the formation and growth of $BaCl_2$ inclusions during the crystallization of fluorochlorozirconate glass.[14–20]

In this work, differential thermal analysis (DTA), XRD† and ^{35}Cl NMR‡ methods were applied to study the crystallization of erbium-doped fluorochlorozirconate glass after isothermal heat treatment during different time intervals. For this purpose, the glass samples, $58ZrF_4{\cdot}10BaF_2{\cdot}10BaCl_2{\cdot}2LaF_3{\cdot}3AlF_3{\cdot}17NaF$ and (doped by 5 mol% of ErF_3) $58ZrF_4{\cdot}10BaF_2{\cdot}10BaCl_2{\cdot}2LaF_3{\cdot}3AlF_3{\cdot}17NaF + 5ErF_3$, were prepared by the technique described in our earlier work[24] (for details, see Online Supplementary Materials). Erbium doping was performed in order to accelerate the relaxation required for measuring NMR spectra. The DTA of the glass sample was carried out in the temperature range of 20–570 °C at a heating rate of 10 °C min^{-1}.[13] Heat treatment was carried out in argon flow at 320 °C for 15 min, 1 h and 3 h. The phase composition of the samples after heat treatment was studied using XRD. The ^{35}Cl NMR spectra of glass samples, including those activated by 5 mol% of ErF_3, were recorded before and after heat treatment. The samples in the form of rods weighing 2 g, 5 mm high and 5 mm in diameter were used for measuring the NMR spectra.

Two exothermic crystallization peaks for the glass sample $58ZrF_4{\cdot}10BaF_2{\cdot}10BaCl_2{\cdot}2LaF_3{\cdot}3AlF_3{\cdot}17NaF$ were detected from the DTA data. The first weak peak T_{x1} at 316 °C is a distinctive feature of fluorochlorozirconate glass containing barium chloride.[9,15] The large crystallization peak at 342 °C is associated with the crystallization of the fluoride glass matrix. The values of the other characteristic glass temperatures are the following: glass transition temperature T_g is 260 °C and melting onset temperature T_m is 424 °C. To obtain glass–crystalline samples containing a chloride phase, the heat treatment temperature close to T_{x1} was chosen.

† X-ray diffraction patterns of the samples were measured at 2θ ranging from 10 to 60° on a diffraction Bruker D8 Advance powder diffractometer (Ni-filtered, Cu$K\alpha$ radiation, LYNXEYE detector) at room temperature. Identification of the obtained samples was performed within the DIFFRAC.EVA (Bruker) software package using the ICDD PDF-2 database.

‡ ^{35}Cl NMR spectra were recorded in a constant magnetic field of 5.50307 T at a temperature of 85 K using a significantly upgraded Bruker MSL[21] spectrometer. The standard Hahn spin echo method with a pulse sequence $\pi/2$–π was used. The frequency sweep spectra were obtained by Fourier transform of the second half of the spin echo followed by crosslinking at equidistant frequency points.[22,23] The rate of nuclear spin–lattice relaxation $1/T_1$ was measured by the saturation recovery method.

An amorphous halo was observed in the diffraction pattern of $58ZrF_4{\cdot}10BaF_2{\cdot}10BaCl_2{\cdot}2LaF_3{\cdot}3AlF_3{\cdot}17NaF + 5ErF_3$ glass sample [Figure 1(*a*)]. Low intensity peaks corresponding to the crystalline phases of monoclinic $BaZr_2F_{10}$, orthorhombic BaF_2 and hexagonal $BaCl_2$ appeared after heat treatment at 320 °C for 15 min [Figure 1(*b*)]. Extending the heat treatment time results in the increased content of the formed crystalline phases in the sample [Figure 1(*c*),(*d*)]. As it was shown earlier,[1,13,15] the first crystalline phases formed during heat treatment of the fluorochlorozirconate and fluorochlorohafnate glass with high $BaCl_2$ concentration (20 mol%) near the first crystallization peak T_{x1} constitute the crystals of hexagonal and orthorhombic $BaCl_2$. However, as observed by TEM,[16] the formation of $BaCl_2$ crystals in glass ceramics was concurrent with the formation of BaF_2 crystals. Both $BaCl_2$ and BaF_2 crystals can be the nucleation centers during the early stages of heat treatment to form $BaZr_2F_{10}$ or β-$BaZrF_6$ crystalline phases. The lower $BaCl_2$ concentration in glass composition may also result in the simultaneous crystallization of the fluoride and chloride phases. XRD patterns of the doped samples, heat-treated under these conditions, did not show the presence of erbium-containing phases.

The ^{35}Cl NMR spectra of both glass and glass ceramics represent the broadened single lines with a broad maximum near the Larmor frequency without any distinguishable quadrupole features (Figure 2). For comparison, the spectrum of polycrystalline hexagonal $BaCl_2$ (Figure 2, spectrum *6*) demonstrates a significantly narrower intensity distribution, which is natural for a crystalline sample. Its simulation gives an estimate of the quadrupole splitting C_q ~1.4 MHz and a fairly high asymmetry parameter ~0.9, which agrees well with the data for similar $CaCl_2$.[25]

Figure 3 shows the dependence of the full width at half maximum of the line (FWHM) on the heat treatment time of erbium-doped glass, and the value of FWHM for matrix glass is noted. The values of the spin–lattice relaxation rate $1/T_1$ for both samples are also given. The addition of magnetic ions Er^{3+} significantly accelerates the relaxation, which is expected as a result of the appearance of an additional relaxation mechanism on magnetic centers.[26] Since in all relaxation measurements it was

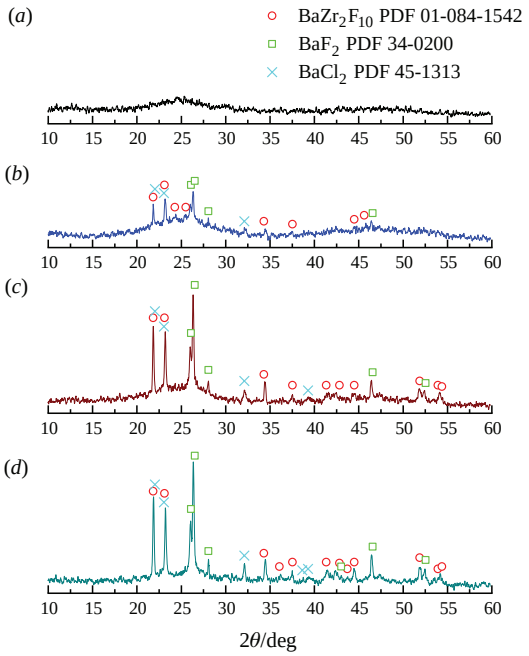

Figure 1 XRD patterns of the samples: (*a*) glass and glass ceramics obtained by heat treatment at 320 °C for (*b*) 15 min, (*c*) 1 h and (*d*) 3 h.

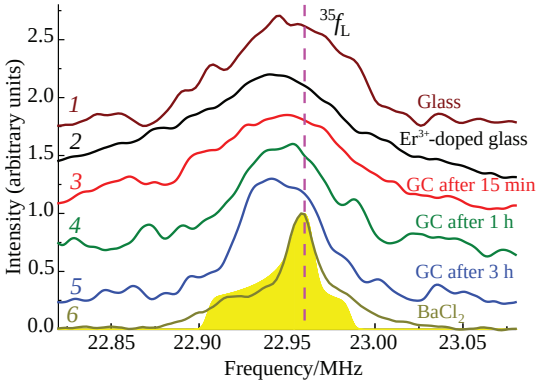

Figure 2 ^{35}Cl NMR spectra of $58ZrF_4{\cdot}10BaF_2{\cdot}10BaCl_2{\cdot}2LaF_3{\cdot}3AlF_3{\cdot}17NaF$ (spectrum *1*, glass) and $58ZrF_4{\cdot}10BaF_2{\cdot}10BaCl_2{\cdot}2LaF_3{\cdot}3AlF_3{\cdot}17NaF + 5ErF_3$ (spectrum *2*, Er^{3+}-doped glass) glasses, doped glass-ceramics (spectra *3*–*5*, GC) and $BaCl_2$ samples (spectrum *6*). The vertical dashed line indicates the Larmor field $^{35}f_L$ of the ^{35}Cl nuclei. The spectra baselines are located at levels 1.7, 1.2, 0.9, 0.6, 0.3 and 0 for samples *1*–*6*, respectively. The heat treatment duration is indicated for each spectrum. Yellow region corresponds to the simulation of the $BaCl_2$ spectrum.

mainly the central transition –½ ↔ ½ that was excited, the recovery curves were approximated by the following relationship: $I = I_0 + (I_{max} - I_0)\{1 - 0.9\exp(-\tau/T_1) - 0.1\exp[-\tau/(6T_1)]\}$,[27] where τ is the time elapsed after the saturating sequence and I_0 and I_{max} are approximating parameters corresponding to the minimum and maximum intensities. The inset in Figure 3 shows the relaxation curves for polycrystalline $BaCl_2$ and activated glass demonstrating the slowest and fastest relaxation, together with the corresponding approximations.

Also, the activation of glass with erbium results in the sizeable broadening of the NMR line (Figure 2), which can be assigned to the magnetic shifts caused by the local fields from Er^{3+}. Low concentration and disordered distribution of both erbium and chlorine in the glass yeilds a dispersion of such shifts comparable to their absolute values. In this case, the characteristic values of local fields can be estimated as FWHM/$^{35}\gamma$ ~0.03 T, which is small for a magnet, but seems realistic for highly scattered magnetic centers.

Subsequent decrease of the line width and relaxation rate during heat treatment of the glass may be due to two reasons. First, chlorine atoms gradually diffuse towards the $BaCl_2$ crystallization grains, so that the characteristic Er–Cl distance increases, and ^{35}Cl nuclei are less and less affected by the magnetic centers. Second, the values of both the relaxation rate and the FWHM eventually become smaller than those for the matrix glass, which points to the influence of still another factor, namely the formation of a structural order. Crystallization, on the one hand, results in the partial ordering in the distribution of the ^{35}Cl electric field gradient and in the narrowing of the NMR line, and on the other hand, to a decrease in the probability of relaxation on defects. At the same time, the line width achieved after three hours of heat treatment is still about twice as wide as that for polycrystalline $BaCl_2$ (24 kHz), and the spin–lattice relaxation rate is about 20 times higher (0.014 s^{-1} for $BaCl_2$). This is not surprising, given that there are no Er^{3+} magnetic ions in $BaCl_2$, although some contribution of chlorine nuclei with low-symmetric environment at the crystallization grain boundary and outside them cannot be completely excluded either. It follows that during crystallization of the glass Er^{3+} ions are redistributed in the bulk glass sample and Er^{3+} ions are mainly displaced from the chloride environment into the fluoride environment. That is consistent with the results[17] demonstrating that the short-wave shift of the Er^{3+} emission lines during heat treatment of the fluorochlorozirconate glass was associated with erbium ion displacement into a fluoride phase.

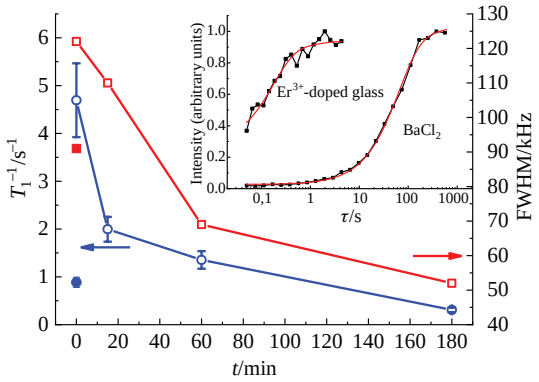

Figure 3 The ^{35}Cl NMR spectra FWHM (empty red squares, right scale) and relaxation rate $1/T_1$ (empty blue circles, left scale) *vs.* the heat treatment time of glass $58ZrF_4{\cdot}10BaF_2{\cdot}10BaCl_2{\cdot}2LaF_3{\cdot}3AlF_3{\cdot}17NaF + 5ErF_3$. The parameters for glass $58ZrF_4{\cdot}10BaF_2{\cdot}10BaCl_2{\cdot}2LaF_3{\cdot}3AlF_3{\cdot}17NaF$ are marked with similar filled symbols. Inset: relaxation curves of individual samples (connected black squares) and their approximations (red curves).

In summary, it has been shown for the first time how ^{35}Cl NMR spectroscopy in combination with DTA and XRD can be used in the study of the fluorochlorozirconate glass crystallization. It was found that during crystallization Er^{3+} cations are displaced into the fluoride phase. The information on crystallization behavior can be used in the development of optimal conditions for obtaining erbium-doped fluorochlorozirconate glass ceramics with specified luminescent properties.

This work was supported by the Ministry of Science and Higher Education of the Russian Federation as part of the State Assignment of Lebedev Physical Institute of the Russian Academy of Sciences, Lomonosov Moscow State University, Kurnakov Institute of General and Inorganic Chemistry of the Russian Academy of Sciences and Prokhorov General Physics Institute of the Russian Academy of Sciences. This research was performed using the equipment of the JRC PMR LPI RAS, MSU, IGIC RAS, GPI RAS.

Online Supplementary Materials

Supplementary data associated with this article can be found in the online version at doi: 10.1016/j.mencom.2024.10.042.

References

1 C. Paßlick, O. Müller, D. Lützenkirchen-Hecht, R. Frahm, J. A. Johnson and S. Schweizer, *J. Appl. Phys.*, 2011, **110**, 113527; https://doi.org/10.1063/1.3662148.
2 L. Zhang, Q. Zhu, Y. Jiang, Z. Wang, X. Yuan, H. Li, H. Chang, S. Cui, L. Wang and L. Zhang, *Ceram. Int.*, 2019, **45**, 4431; https://doi.org/10.1016/j.ceramint.2018.11.121.
3 M. N. Brekhovskikh, S. Kh. Batygov, L. V. Moiseeva, L. I. Demina, V. V. Vinokurova and L. A. Vaimugin, *Mendeleev Commun.*, 2023, **33**, 525; https://doi.org/10.1016/j.mencom.2023.06.027.
4 H. Jin, Z.-J. Mo, X.-Z. Zhang, L.-L. Yuan, M. Yan and L. Li, *Chin. Phys. B*, 2016, **25**, 103201; https://doi.org/10.1088/1674-1056/25/10/103201.
5 C. Yu, J. Zhang, G. Wang and Z. Jiang, *J. Alloys Compd.*, 2008, **461**, 378; https://doi.org/10.1016/j.jallcom.2007.06.096.
6 G. Chen, J. Johnson, R. Weber, R. Nishikawa, S. Schweizer, P. Newman and D. MacFarlane, *J. Non-Cryst. Solids*, 2006, **352**, 610; https://doi.org/10.1016/j.jnoncrysol.2005.11.048.
7 A. Edgar, G. V. M. Williams, S. Schweizer and J.-M. Spaeth, *Curr. Appl. Phys.*, 2006, **6**, 399; https://doi.org/10.1016/j.cap.2005.11.027.
8 A. W. Evans, R. L. Leonard, S. K. Gray, J. E. King, A. R. Lubinsky and J. A. Johnson, *J. Non-Cryst. Sol.*, 2018, **484**, 8; https://doi.org/10.1016/j.jnoncrysol.2018.01.015.
9 B. Henke, C. Paßlick, P. Keil, J. A. Johnson and S. Schweizer, *J. Appl. Phys.*, 2009, **106**, 113501; https://doi.org/10.1063/1.3259390.
10 R. L. Leonard, A. R. Lubinsky and J. A. Johnson, *J. Am. Ceram. Soc.*, 2017, **100**, 1551; https://doi.org/10.1111/jace.14681.
11 B. Ahrens, S. Brand, T. Büchner, P. Darr, S. Schoenfelder, C. Paßlick and S. Schweizer, *J. Non-Cryst. Solids*, 2011, **357**, 2264; https://doi.org/10.1016/j.jnoncrysol.2010.11.084.
12 G. Okada, A. Edgar, S. Kasap and T. Yanagida, *Jpn. J. Appl. Phys.*, 2016, **55**, 02BC07; https://doi.org/10.7567/JJAP.55.02BC07.
13 S. Kh. Batygov, M. N. Brekhovskikh, L. V. Moiseeva and R. M. Zakalyukin, *Inorg. Mater.*, 2020, **56**, 1290; https://doi.org/10.1134/S0020168520120031.
14 G. Soundararajan, C. Koughia, A. Edgar, C. Varoy and S. Kasap, *J. Non-Cryst. Solids*, 2011, **357**, 2475; https://doi.org/10.1016/j.jnoncrysol.2010.11.053.
15 M. N. Brekhovskikh, L. V. Moiseeva, V. E. Shukshin, I. A. Zhidkova, A. V. Egorysheva and V. A. Fedorov, *Inorg. Mater.*, 2019, **55**, 173; https://doi.org/10.1134/S0020168519020018.
16 C. J. Alvarez, Y. Liu, R. L. Leonard, J. A. Johnson and A. K. Petford-Long, *J. Am. Ceram. Soc.*, 2013, **96**, 3617; https://doi.org/10.1111/jace.12540.
17 M. N. Brekhovskikh, B. I. Galagan, L. N. Dmitruk, L. V. Moiseeva and V. A. Fedorov, *Inorg. Mater.*, 2009, **45**, 579; https://doi.org/10.1134/S0020168509050215.
18 M. P. Shepilov, *Opt. Mater.*, 2008, **30**, 839; https://doi.org/10.1016/j.optmat.2007.03.004.
19 C. Paßlick, J. A. Johnson and S. Schweizer, *J. Non-Cryst. Solids*, 2013, **371**–**372**, 33; https://doi.org/10.1016/j.jnoncrysol.2013.03.042.
20 U. Skrzypczak, C. Pfau, C. Bohley, G. Seifert and S. Schweizer, *J. Non-Cryst. Solids*, 2013, **363**, 205; https://doi.org/10.1016/j.jnoncrysol.2012.12.039.
21 S. V. Zhurenko, A. V. Tkachev, A. V. Gunbin and A. A. Gippius, *Instrum. Exp. Tech.*, 2021, **64**, 427; https://doi.org/10.1134/S0020441221020202.
22 A. P. Bussandri and M. J. Zuriaga, *J. Magn. Reson.*, 1998, **131**, 224; https://doi.org/10.1006/jmre.1998.1363.
23 W. G. Clark, M. E. Hanson, F. Lefloch and P. Ségransan, *Rev. Sci. Instrum.*, 1995, **66**, 2453; https://doi.org/10.1063/1.1145643.
24 M. N. Brekhovskikh, S. Kh. Batygov, L. V. Moiseeva, A. V. Egorysheva and V. A. Fedorov, *Inorg. Mater.*, 2016, **52**, 63; https://doi.org/10.1134/S0020168516010027.
25 T. O. Sandland, L.-S. Du, J. F. Stebbins and J. D. Webster, *Geochim. Cosmochim. Acta*, 2004, **68**, 5059; https://doi.org/10.1016/j.gca.2004.07.017.
26 T. Moriya, *Spin Fluctuations in Itinerant Electron Magnetism*, Springer, Berlin, 1985; https://doi.org/10.1007/978-3-642-82499-9.
27 A. Narath, *Phys. Rev.*, 1967, **162**, 320; https://doi.org/10.1103/PhysRev.162.320.

Received: 6th June 2024; Com. 24/7528